Article

Variable Electronic Coupling in Phenylacetylene Dendrimers: The Role of Förster, Dexter, and Charge-Transfer Interactions

Alexis L. Thompson, Kevin M. Gaab, Jianjun Xu, Christopher J. Bardeen, and Todd J. Martnez

J. Phys. Chem. A, **2004**, 108 (4), 671-682 • DOI: 10.1021/jp030953u

Variable Electronic Coupling in Phenylacetylene Dendrimers: The Role of Förster, Dexter, and Charge-Transfer Interactions

Alexis L. Thompson, Kevin M. Gaab, Jianjun Xu, Christopher J. Bardeen,* and Todd J. Martínez*

Department of Chemistry, University of Illinois at Urbana-Champaign, 600 South Mathews Avenue, Urbana, Illinois 61801

Received: July 31, 2003; In Final Form: October 31, 2003

A combination of theory and experiment is used to identify a novel variable excitonic coupling in a series of building blocks for small phenylacetylene dendrons. Systematic changes in the experimental emission spectra, radiative lifetimes, and polarization anisotropies as the number of meta-conjugated branches increases provide evidence for a qualitative change in the electronic structure in the relaxed excited state. The excited state electronic structure is investigated theoretically using ab initio CASSCF and CASPT2 calculations, which indicate the presence of large electronic coupling in the emitting geometry that is not seen for the absorbing geometry of the same molecules. The changes in electronic structure that occur upon excited-state relaxation can be understood in terms of a variable excitonic coupling between the phenylactylene branches, which takes these molecules from the weak coupling to the strong coupling regime as they relax on the excited state. The origin of this geometry-dependent coupling is investigated through the interpretation of ab initio calculations in terms of Förster, Dexter, and through-bond charge-transfer interactions. We find that the change in the coupling arises primarily from an increase in the through-bond or charge-transfer component of the coupling, despite the absence of large changes in charge distribution. A theoretical comparison of meta- versus para-substituted phenylacetylenes clarifies why this effect is so pronounced in the meta-substituted molecules.

Introduction

Conjugated organic molecules have attracted considerable attention for use in applications such as electroluminescence and solar energy conversion. In particular, conjugated dendrimers have been proposed as the light-harvesting component of synthetic solar energy converters, since their multichromophoric structure is analogous to that of light-harvesting complexes (LHCs) found in biological systems.[1] These dendrimers consist of covalently linked networks of chromophores, where electronic energy deposited at one site in the supermolecule can be transferred among the chromophores until it reaches a single low-energy site. At this "trap" site, the photon energy can then be used to drive a chemical process such as charge separation that creates useful work. The efficiency of this energy conversion process depends critically on facile interchromophore energy transfer. This transfer has been studied both theoretically and experimentally in a variety of systems,[2,3] and its dynamics are determined by the magnitude of the interchromophore coupling term, V. Chromophore−chromophore interactions in these systems can be classified according to two limits: strong coupling (coherent transfer) and weak coupling (incoherent transfer).[4,5] In the limit of strong coupling, the energy cycles back and forth coherently between the chromophores due to delocalized excitonic states created by the nonnegligible V term in the system Hamiltonian. In the weak coupling limit, V is smaller than the electronic dephasing of the system, which is due to environmental fluctuations such as collisions and vibrations. In this limit, the absorption and emission spectra are unchanged since V is not large enough to measurably perturb the broadened electronic line shapes. An intermediate regime can also be envisioned, where some subsets of the chromophores are strongly coupled and these subsets are weakly coupled to each other. Such a situation appears to hold in the case of the bacterial LHC, where the excitation is delocalized over two to four of the constituent chlorophylls,[6−8] even though these are not covalently linked.

Many workers have studied conjugated absorbers connected by sp^3-hybridized linker groups, where the covalent linkers are electronically distinct from the chromophores.[9−15] In these systems, most of the experimental observables are well-described by Förster transfer between weakly coupled absorbers, although there is also evidence for coherent energy transfer in at least one such system.[16] Dendrimers in the strong coupling limit, where faster energy transfer is in principle possible, have been the subject of far fewer studies.[17−19]

In the current paper, we examine a system that had previously been assumed to be in the weak coupling limit,[19−21] namely, the meta-conjugated phenylacetylene (PA) dendrimers first synthesized by Moore and co-workers.[22] These molecules are of particular interest due to their high light-harvesting efficiencies and compact structure. Their compact structure is because the chromophores serve as the linkers as well: the entire structure is conjugated. The molecules shown in Figure 1, which are the building blocks of the larger PA dendrimers studied by Moore and co-workers, are the subject of the experimental and theoretical work described here. These "dendrons" or fragments of dendrimeric macromolecules show absorption properties that are consistent with weakly coupled diphenylacetylene (DPA)

10.1021/jp030953u CCC: $27.50
Published on Web 01/03/2004

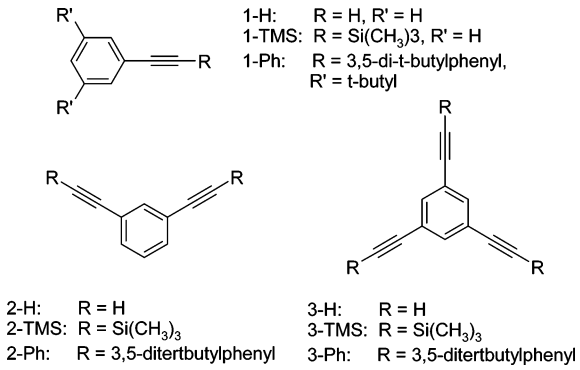

Figure 1. Phenylacetylene compounds examined in this work.

subunits. However, their emission spectral shapes, radiative lifetimes, and polarization anisotropies undergo dramatic changes with increasing size, suggesting strongly coupled DPA units. To understand the origin of these changes, we turn to high-level electronic structure calculations. The level shifts and reordering obtained from these ab initio calculations show qualitative agreement with an intramolecular excitonic model where the coupling between the PA segments varies with nuclear geometry. The variable electronic coupling, which we have communicated recently,[23] is due to a combination of through-space and through-bond interactions between the PA arms connected through a central phenyl ring. Using theoretical calculations on different conjugated systems, Bredas and co-workers have observed minor effects, attributed to through-space interactions, on interchromophore coupling due to excited-state relaxation.[24] However, to the best of our knowledge, such large variability in the electronic coupling as that reported here has not been previously observed. We analyze these interactions quantitatively by recasting the ab initio results in terms of a model developed by Harcourt et al.,[25] which classifies the different types of interactions between electronically coupled chromophores. We find that the variation of the electronic coupling V with molecular geometry is due to the through-bond or charge-transfer type of interaction rather than the more familiar dipole−dipole and Dexter terms. Our results demonstrate that even subtle changes in the electronic orbital structure, as embodied in the charge-transfer analysis, can dramatically change the excitonic coupling of covalently linked conjugated chromophores. The relative roles of the three interaction terms and their dependence on meta- versus para-substitution is investigated in detail. Our findings are a first step toward a comprehensive conceptual framework within which to understand electronic dynamics in these conjugated networks.

Experiment and Methods

The syntheses of the phenyl- and trimethylsilyl (TMS)-terminated derivatives of **1**, **2**, and **3**, shown in Figure 1, are accomplished by the Sonagashira palladium-catalyzed coupling of di-*tert*-butylphenylacetylene to an aromatic mono-, di-, or trihalide (bromide or iodide), respectively, as described by Xu et al.[26] **1-H**, **2-H** (GFS Chemicals), and **3-H** (Alfa Aesar) are obtained commercially and used as received. Synthesized products are purified by silica gel column chromatography with elution with *n*-hexanes and multiple recrystallizations from 2:1 CH_2Cl_2/methanol solution. The purity of each product is verified by HPLC with a mobile phase of 4:1 *n*-hexanes/CH_2Cl_2. Cyclohexane is used for all room-temperature lifetime and quantum yield measurements, and a 1:3 methylcyclohexane/isopentane mixture is used for the anisotropy measurements at 77 K. The methylcyclohexane is purified as described in the literature.[27]

Steady-state absorption and fluorescence spectra are recorded on an Ocean Optics SD2000 and a Spex FluorMax-2, respectively. Absolute quantum yields are determined relative to *p*-terphenyl using 290 nm excitation and are conducted using highly dilute samples with optical densities less than 0.1. Samples used for quantum yield measurements are dissolved in cyclohexane and deoxygenated prior to use by sonication followed by vigorous bubbling with argon. With the exception of toluene and DMF, which are reagent grade, all other solvents were UV spectroscopic grade and used as received.

Excitation pulses for picosecond time-resolved emission and anisotropy measurements are generated using a home-built noncollinear optical parametric amplifier (NOPA) pumped by the 800 nm output of a 40 kHz Spectra Physics Spitfire regenerative amplifier.[28] For these experiments, the 600 nm NOPA output is frequency doubled to 300 nm using a 0.4 mm BBO. Fluences are less than 5 nJ/cm^2. Samples are mounted in a cryostat using a homemade quartz sample cell and have concentrations of $\sim 2 \times 10^{-5}$ M. Changing the concentration by a factor of 10 does not change the spectra or the dynamics, ruling out aggregation effects. The fluorescence is collected perpendicular to the excitation beam, collimated, and focused into a Spectra Pro-150 spectrometer with a 150 grooves/mm grating to disperse the spectrum before being passed to a Hamamatsu C4334 streak camera. The instrumental response time of this instrument is ~30 ps in a 1 ns sweep window. All fluorescence lifetimes are well-fit with single exponentials. For the fluorescence anisotropy measurements, a calcite polarizer is used to purify the polarization of the excitation beam, while a second calcite polarizer is placed in the collimated emission and rotated relative to the excitation. The integrated emission is detected using a Hamamatsu R7400U PMT and SRS SR830 lock-in amplifier. The anisotropies are measured in a glass at 77 K to remove any rotational depolarization. The spectral and time dependences of the fluorescence anisotropy

$$r(\lambda,t) = (I_{||}(\lambda,t) - I_{\perp}(\lambda,t))/(I_{||}(\lambda,t) + 2I_{\perp}(\lambda,t)) \qquad (1)$$

are examined using the streak camera setup and determined to be constant for all emission wavelengths on the nanosecond time scale. Measurement of the anisotropy of *p*-terphenyl gives a value of 0.30, in reasonable agreement with the literature value of 0.33.[29]

The ab initio calculations are performed using the MOLPRO[30] suite of electronic structure codes unless otherwise noted. For all theoretical work, the **(1−3)-Ph** series is modeled without the *tert*-butyl groups, which are not expected to have much effect on the results reported here. State-specific and state-averaged complete active space self-consistent field (CASSCF)[31−33] methods are used. The number of states used in the state-averaged CASSCF calculations is chosen to average over the fewest number of states while describing all of the low-lying bright states of interest. All states included in the average are equally weighted. The number of states included in the average, as well as the size of the active space, varies for the different molecules according to the criterion that the lowest-lying bright states be well-described. The state-averaged CASSCF calculations are referred to as SA-*N*-CASSCF(n/m) where N is the number of states averaged in the calculation, n is the number of active electrons, and m is the number of active orbitals. The single-point calculations and optimizations are run without symmetry constraints, and all orbitals are optimized unless otherwise mentioned. Calculations use the 6-31G basis set,[34]

except where otherwise noted. The absorbing state is taken to be the lowest lying bright state in the excited state manifold of the optimized ground state geometry. The lowest lying excited state with significant oscillator strength at the relaxed excited state geometry is the emitting state. Dynamic electron correlation, especially important for vertical excitation energies, is accounted for where feasible by performing an internally contracted complete active space second-order perturbation theory (CASPT2)[35,36] calculation using the same state-averaging and active spaces as those used for the CASSCF calculation. These CASPT2 calculations are only possible on **(1−3)-H** due to the large size of the phenyl-terminated molecules.

Ground state geometries for **(1−3)-Ph** are obtained with B3LYP-DFT in the 6-31G** basis set[37] as implemented in Jaguar[38] without the use of symmetry. Single-point CASSCF calculations on these molecules are run using C_s symmetry, and the carbon 1s orbitals are not optimized. Energies and state orderings are calculated using single-point CASSCF calculations as described above. In the calculations performed to elucidate the nature of the variable excitonic coupling in **1-Ph** and **2-Ph**, we use an active space with four electrons and orbitals for each phenyl ring. The absorbing and emitting geometries of **2-Ph** are optimized using CASSCF with C_{2v} symmetry.

The natural orbitals from CASSCF calculations comprise just one of many equivalent sets of orbitals. Any linear combination, that is, unitary transformation, of orbitals within the active space can be taken without affecting the final wave function or energy. The orbitals that result from CASSCF calculations on the molecules that we study here are generally delocalized and thus not ideal for understanding the origin of the excitonic states in terms of localized chromophores. Thus, in section 4, when we calculate the various types of coupling in the PA dendrimers, we exploit this property of CASSCF orbitals to construct orbitals localized on each of the two chromophores in **2-Ph**. The CASSCF orbitals are orthogonal, and this orthogonality is maintained under unitary rotations. Therefore, the localized orbitals have "orthogonalization tails", which prevent the orbitals from being strictly localized on one of the two DPA chromophores. However, a quantitative assessment of the amount of each localized orbital that extends on the most distant phenyl ring shows that this is negligible—in all cases, more than 99% of the orbital density is on one of the DPA subunits. These localized orbitals are used to interpret the results in terms of an exciton model similar to that developed by Harcourt et al.[25] To compare the results of the meta-substituted **2-Ph** molecule with a para-substituted analogue, we examine 1,4-bis(phenylethynyl)-benzene (**P2-Ph**). The geometries are optimized using C_s symmetry, which is maintained in the subsequent CASSCF calculations.

Results

1. Spectroscopy of Phenylacetylene Dendrons. The normalized steady-state absorption spectra of the compounds in Figure 1 are shown in Figure 2a. Progressing through the series from compounds **1-Ph** to **3-Ph**, there are only modest changes in the absorption spectra. Most notably, there is a ∼640 cm^{-1} red shift of the lowest energy peak. Additionally, there is a rearrangement of relative intensity with the red edge of the absorption gaining intensity relative to the blue. The structure of the spectra, however, remains largely unchanged. This lack of shifting in the absorption spectra is also seen for much larger PA dendrimers.[20] In contrast to the absorption spectra, there are dramatic changes in the emission spectra of **1-Ph**, **2-Ph,** and **3-Ph**, as seen in Figure 2b. The 0−0 peak of the fluorescence

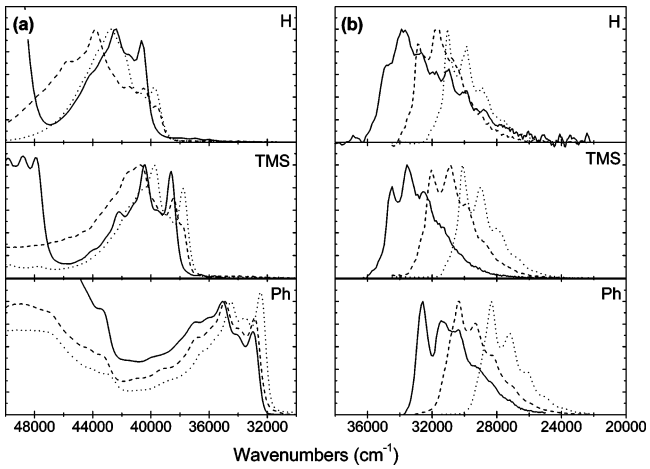

Figure 2. The steady-state absorption (a) and emission (b) spectra for **1** (—), **2** (− − −), and **3** (···) with various terminal groups, as depicted in Figure 1.

shifts from ∼32 600 cm^{-1} in **1-Ph** to ∼30 400 cm^{-1} in **2-Ph**, a shift of ∼2200 cm^{-1}. A further shift of ∼2100 cm^{-1} is observed in **3-Ph**, the maximum occurring at ∼28 300 cm^{-1}. For dendrimers larger than **3-Ph**, however, the emission spectra do not experience any further shifts.[22,39]

To determine the generality of this size effect on the fluorescence spectrum, we also examined the smaller hydrogen and TMS analogues shown in Figure 1. Changing the acetylene terminal groups from phenyl to hydrogen or TMS has very little impact on the qualitative behavior of the steady-state spectra, as shown in Figure 2. Although changing this end group does result in an absolute shift of the absorption, from ∼33 000 cm^{-1} in the **Ph**-terminated to ∼40 000 cm^{-1} in the **H**-terminated, within a given series there consistently remains very little red shift with additional substitution on the central phenyl. Strikingly, the absolute position of fluorescence is shifted much less than the absorption with **1-H** at ∼34 700 cm^{-1}, **1-TMS** at ∼34 500 cm^{-1}, and **1-Ph** at ∼32 600 cm^{-1}. Furthermore, the relative shifts from **1** to **3** remain relatively constant at ∼3700 cm^{-1} for **H**, ∼4400 cm^{-1} for **TMS**, and ∼4200 cm^{-1} for the **Ph**-terminated series. Because of low quantum yield and rapid falloff in the excitation source intensity near 40 000 cm^{-1}, the emission spectrum of **1-H** exhibits lower signal-to-noise (although still acceptable for our purposes) than the other compounds studied. A comparison of the experimental Stokes shift, given here by

$$\Delta\nu_{ss} = \nu_{0-0}^{abs} - \nu_{0-0}^{em} \qquad (2)$$

where 0−0 denotes the first peak in the vibronic progression, for the −H, −TMS, and −Ph series shows that the Stokes shift increases by about 2000 cm^{-1} for each step in the series. Because the qualitative trends remain consistent with substitution of the acetylene terminal group, we believe that the basic photophysics of all three series are similar.

Table 1 summarizes the changes in the excited-state dynamics observed for **(1−3)-Ph**. There is an increase in the fluorescence quantum yield (ϕ_{fl}) from 5.5×10^{-3} for **1-Ph** to 0.19 for **2-Ph** to 0.35 for **3-Ph**. As has been observed previously for unsubstituted DPA, the fluorescence lifetime and quantum yield of **1-Ph** are strongly temperature-dependent. This may be due to a barrier separating the Franck−Condon geometry and an avoided crossing or conical intersection involving either a second excited state or the ground state.[40−42] At 77 K, its fluorescence lifetime is 0.62 ns with a quantum yield of 0.50. The measured

TABLE 1: Photophysical Parameters for Phenyl-Terminated Dendrons

	nondeaerated			deaerated					Strickler−Berg		Stokes
	Φ_{fl}(298K)	τ_{fl}(298K), ns	τ_{rad}, ns	Φ_{fl}(298K)	τ_{fl}(298K), ns	Φ_{fl}(77K)	τ_{fl}(77K), ns	τ_{rad}, ns	τ_{rad}, ns	R_0	shift, cm^{-1}
1-Ph	0.0055	<0.050	<9	0.0055	<0.050	0.50	0.62	1.2	1.4	0.30	500
2-Ph	0.15	4.6	31	0.19	5.4		11.3	28	0.79	0.24	2400
3-Ph	0.24	11.2	46	0.35	14.9		26.5	43	0.72	0.12	4100

fluorescence lifetimes and quantum yields of **2-Ph** and **3-Ph** increase relative to **1-Ph**, and these two quantities determine the radiative lifetime via the relation

$$\tau_{rad} = \frac{\tau_{fl}}{\phi_{fl}} \quad (3)$$

Using the values in Table 1, we find radiative lifetimes of 1.2, 28, and 43 ns for this series of compounds in deaerated solution. For samples that were not deaerated, we obtain very similar radiative lifetimes. For **1-Ph**, this is in good agreement with that observed previously for unsubstituted DPA (1.2 ns)[41] and is close to the rate of 1.4 ns determined by the Strickler−Berg equation, which relates the radiative lifetime of the fluorescence to the integrated absorption:

$$k_r^{SB} = (2.88 \times 10^{-9}) n^2 \frac{g_l}{g_u} \frac{\int I(\tilde{\nu}_F)\, d\tilde{\nu}_F}{\int \tilde{\nu}_F^{-3} I(\tilde{\nu}_F)\, d\tilde{\nu}_F} \int \frac{\epsilon(\tilde{\nu})}{\tilde{\nu}}\, d\tilde{\nu} \quad (4)$$

where ϵ is the molar extinction coefficient in $cm^{-1}\ M^{-1}$, $I(\nu)$ is the normalized emission spectrum, and the limits in the integrals are in the present case taken to be $22\,000 < \tilde{\nu} < 42\,000\ cm^{-1}$, consistent with the relevant absorption band in these molecules. For these calculations, the degeneracy factor g_l/g_u was taken to be unity. For **2-Ph** and **3-Ph**, the radiative lifetimes are more than a factor of 10 larger than that of **1-Ph** and than those predicted by a Strickler−Berg calculation. Last, the anisotropies are different for the three molecules. The initial fluorescence anisotropy of **1-Ph** is 0.30, which is close to 0.40, the expected value if the absorbing and emitting states have the same transition dipole moment direction.[43] However, the initial anisotropies for dendrons **2-Ph** and **3-Ph** are considerably lower than that of **1-Ph**, 0.23 and 0.12, respectively.

2. Calculations of Ground and Excited States of Phenylacetylene Dendrons. To better understand the photophysics of the PA dendrons, we use high-level ab initio theory to calculate the absorbing and emitting states. The accuracy and reliability of the method is probed by determining whether it can reproduce the experimental spectra and Stokes shifts. Calculations done on the **(1−3)-H** and the **(1−3)-Ph** molecules show very similar patterns in the excited-state behavior. The results obtained with a large active space CASSCF calculation on **1-Ph** and **2-Ph** show the same lack of shift in the absorption energies and the same excited state orderings as those seen in **(1−3)-H** at the CASPT2 level of theory. This correspondence, along with the similarities seen in the experimental spectra (Figure 2), allows us to focus on the behavior of the smaller **(1−3)-H** series where we are able to use higher levels of theory including dynamic electron correlation. To determine the nature of the absorbing and emitting states of these molecules, the relaxed ground and excited state geometries are found using SA-3-CASSCF(4/4) for **1-H**, SA-4-CASSCF(4/4) for **2-H**, and SA-7-CASSCF(6/6) for **3-H**. To obtain the most accurate values for the state energies, we use the results at the CASPT2 level of theory. The same active spaces are used as in the CASSCF optimizations, and the carbon 1s orbitals are left uncorrelated. The CASPT2 calculation for **3-H** is done in C_s symmetry. Level shifts of 0.1 and 0.3 au are used for **1-H** and **3-H**, respectively.

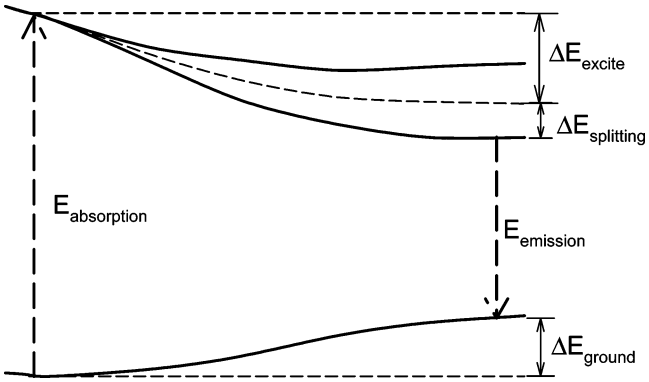

Figure 3. Diagram showing the contribution to the Stokes shift from different changes in the potential energy surfaces of a molecule.

TABLE 2: Components of Stokes Shifts (cm^{-1}) as Calculated Using CASPT2 and Comparison of the Total CASPT2 Stokes Shifts with Experiment[a]

	1-H	**2-H**	**3-H**
ΔE_{ground}	816	675	3416
ΔE_{excite}	4228	2792	594
$\Delta E_{splitting}$	0	1986	3130
CASPT2 Stokes shift	5044	5453	7139
exptl. Stokes shift	5928	6788	8627

[a] See text for details.

The observed Stokes shift corresponds to the difference in energy between the absorption and the emission. Three major changes to the potential energy surfaces of the molecule can lead to this energy difference. A sketch of these effects is shown in Figure 3. The first is the increase in the energy of the ground state as the molecule relaxes to the emitting geometry, which contributes a value ΔE_{ground} to the Stokes shift. Second, the excited-state energy decreases by ΔE_{excite} for this same geometry change, further lowering the energy difference between electronic states. Finally, if the absorbing states are degenerate, then the states may be split as the molecule relaxes, for example, due to a Jahn−Teller effect.[44] The splitting of the emitting state relative to the lowering of the entire manifold, $\Delta E_{splitting}$, is the final contribution to the Stokes shift. We are able to quantify each of these terms from the ab initio calculations, and these values for **(1−3)-H** are found in Table 2. The relaxation of the excited state decreases with increased conjugation, as is seen in linear alkenes. The destabilization of the ground state as a result of the excited-state relaxation increases from **1-H** to **3-H**, which is likely related to the increased cumulenic distortion of **3-H**. The sum of the absolute values of the C−C bond length changes for **1-H** and **2-H** are 0.31 and 0.27 Å, respectively. The value for **3-H**, however, is 0.50 Å, which could explain the large destabilization of the ground state seen in this molecule.

To quantitatively compare the results of the ab initio calculations with the experimental results, we compare the difference between the absorption and fluorescence energies for

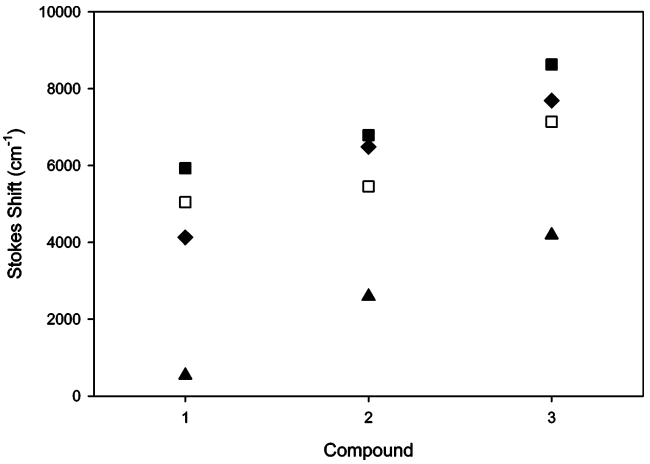

Figure 4. Experimental stokes shifts for H- (■), TMS- (◆), and Ph-terminated (▲) compounds and calculated CASPT2 stokes shifts (□) for the H-terminated series.

each series of molecules. To make the quantitative comparison most accurate, for the ab initio points, we use CASPT2 energies at the CASSCF-minimized geometries. The excitation energies for **(1−3)-H** with CASPT2 are 50 000 ± 2000 cm^{-1} and therefore unchanged across the series within the error of the method. This is consistent with the experimental result in which the absorption maximum shifts by less than 1000 cm^{-1} for the series. Larger basis sets are required for quantitative accuracy in the absolute values of the vertical excitation and emission energies, but our comparison focuses on Stokes shifts, which are less sensitive to basis set effects. For example, the vertical excitation energy of **1-H** is reduced from 6.16 to 5.70 eV when the basis set is enlarged from 6-31G to 6-31G**, compared to the experimental value[45] of ∼5.4 eV. However, this basis set enlargement leads to only a 218 cm^{-1} change in the Stokes shift for **1-H**. Further data concerning calculations using the 6-31G** basis set is available in the accompanying Supporting Information.

The experimental Stokes shift is defined in eq 2. The difference between the vertical excitation energy and the vertical emission energy is used as the theoretical Stokes shift. These energies should be close to the maximum in the experimental absorption or emission spectrum. Figure 4 shows the experimental Stokes shifts for the **−H**, **−TMS**, and **−Ph** series and the calculated CASPT2 Stokes shifts for the **−H** series. The Stokes shifts from the ab initio calculations are in good agreement with the experimental results, with a systematic offset of ∼1000 cm^{-1}.[46]

3. Exciton Model Interpretation of ab Initio Results. The lack of significant spectral shifting or reshaping of the phenylacetylene dendrimer absorption spectra with increasing size led Kopelman and co-workers to conclude that the excitations were localized to the individual dendrimer branches.[20] From the small red shift of the absorption, they set an upper limit of 60 cm^{-1} for the excitonic coupling between segments.[39] The apparent weak coupling of the segments has provided the basis for several analyses of the energy-transfer dynamics in these dendrimers, which assume that Förster energy transfer occurs between effective chromophores centered on different branches of the molecule. If this were actually the case and compound **3-Ph** was equivalent to three symmetrically arranged DPAs, then the emission would be expected to be identical to that of **1-Ph** except for a depolarization due to energy randomization among the three chromophores and a possible red shift due to slight changes in the local dielectric environment. From the data in Figure 2 and Table 1, this is clearly not the case. The large shifts and shape changes in the emission spectra, along with changes in lifetime and oscillator strength, all indicate that the emitting states in **2-Ph** and **3-Ph** are fundamentally different from that in **1-Ph**.

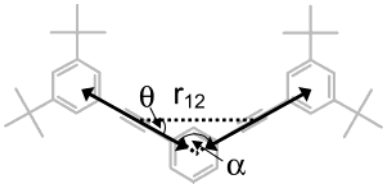

Figure 5. Geometry used for point-dipole exciton calculations.

One mechanism to generate new electronic states with different orientations and oscillator strengths is if the DPA segments of molecules **2-Ph** and **3-Ph** experience strong excitonic coupling.[47] The simplest estimate of the magnitude of such coupling comes from a point-dipole expansion of the transition charge densities and for the geometry shown in Figure 5 leads to

$$V_{\text{point-dipole}} = \frac{|M|^2}{4\pi\epsilon r_{12}^{\,3}}(\cos\alpha + 3\cos^2\theta) \qquad (5)$$

Using the values $r_{12} = 5.89$ Å, $\epsilon = 1.89\epsilon_0$ (for hexane), $\alpha = 120°$, $\theta = 30°$, and $M = 2.65 \times 10^{-29}$ C m,[41] we obtain a coupling of ∼1400 cm^{-1}. Because of the geometry, the value of V diverges when a more rigorous extended dipole method is used.[48,49] For a single excited state, this coupling would be expected to produce large shifts in both the emission and absorption spectra. A way to avoid this is to assume that the absorbing and emitting configurations are so different, either due to relaxation on a single excited state potential energy surface or due to relaxation to a different excited state, that the exciton coupling only affects the emitting state. Even assuming this hypothesis is correct, however, the angle between the two DPA chromophores makes this dimer similar to a J-aggregate and leads to the lower energy state being more strongly allowed in the point dipole approximation.[47] The situation is similar for compound **3-Ph**, and in both cases, we would expect the radiative lifetime to decrease due to the increased oscillator strength, not increase as observed.

The simple point-dipole model discussed above cannot describe our results. Nevertheless, it is worth asking whether these results can be described in terms of an exciton model at all, considering that such models have had some success in describing intramolecular excited states[50,51] and have already been applied to larger PA dendrimers.[18,52−54] To compare an exciton model (with $V < 0$ to make the lower state less-allowed) to the ab initio results, we examine the level ordering and transition dipole moments predicted by each method. The ab initio energy levels and oscillator strengths for **2-H** and **3-H** are shown in Figure 6a. In the ground state relaxed geometry, the absorbing states are nearly degenerate for both molecules, but a significant splitting of these states occurs in the emitting geometry. The relaxed emitting geometry has a cumulenic structure for all of the molecules in the series. In the **2-H** molecule, two degenerate states are seen in the absorbing geometry, corresponding to the number of DPA-like units (in the **−H** series, these are actually phenylacetylene units) present in the molecule. For **3-H**, the absorbing state consists of three nearly degenerate states. For both molecules, as they relax to the cumulenic emitting geometry, the excited states split with

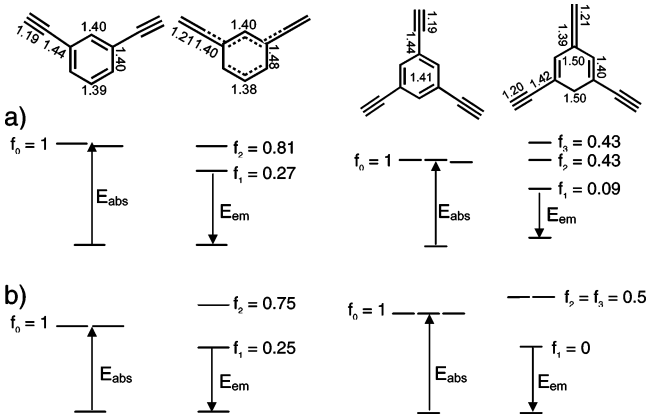

Figure 6. Comparison of energy level structure and oscillator strengths for **2-H** and **3-H** for absorbing and emitting geometries from (a) ab initio calculations and (b) exciton model with variable coupling *V*.

a weakly emissive state lying below states that retain most of the oscillator strength. To map these results onto the predictions of a simple exciton model, the coupling term must be allowed to change from essentially zero in the absorbing geometry to a larger value in the emitting geometry. Later in the manuscript, we will analyze the results of theoretical calculations to see if such an apparently ad hoc prescription is indeed justified. A negative value of the coupling leads to the splitting seen in **2-H**, in which the lower state has less oscillator strength than the upper state, as predicted by ab initio calculations. The energy levels are shown in Figure 6b for **2-H** and **3-H** in which the coupling changes from $V = 0$ (corresponding to the absorbing geometry) to $V < 0$ (corresponding to the emitting geometry). In the exciton model, the only change between the absorbing and emitting calculation is the value of the coupling. The exciton model and the ab initio calculations predict very similar state orderings and relative oscillator strengths. The most noticeable difference is that the exciton model predicts that the upper states in the emitting geometry of **3-H** are degenerate while they are split in the ab initio calculation. This difference is likely due to the decrease in symmetry of the ab initio emitting geometry. Since the simple exciton model that we are considering does not take into account geometry distortions, it cannot correctly reproduce this behavior.

The behavior of these molecules is consistent with a variable coupling between the states as a function of the cumulenic geometric distortion. In the ground state geometry, the coupling is small or nonexistent, but as the molecule relaxes on the excited state, the coupling becomes a large, negative value. This type of geometry-dependent coupling might be explained by a large geometric distortion upon excited state relaxation. This, however, is not the case as seen in Figure 7a, which shows the distortions in the geometry to be primarily changes in bond alternation with bond lengths changing by only several hundredths of an angstrom. Another potential explanation for this type of coupling would be if some of the excited states acquired significant charge-transfer character during their relaxation. Figure 7b shows the changes in the Mulliken charges of each carbon atom at the emitting geometry relative to the ground state of the absorbing geometry. The charges of H atoms have been summed into the C atom to which they are bonded. Again, the changes are not large, indicating that the state is not predominantly charge transfer in character. To confirm the absence of charge-transfer character in these compounds, we examined the solvatochromism of **(1−3)-Ph** in toluene, THF, methylene chloride, and DMF, in addition to cyclohexane. In

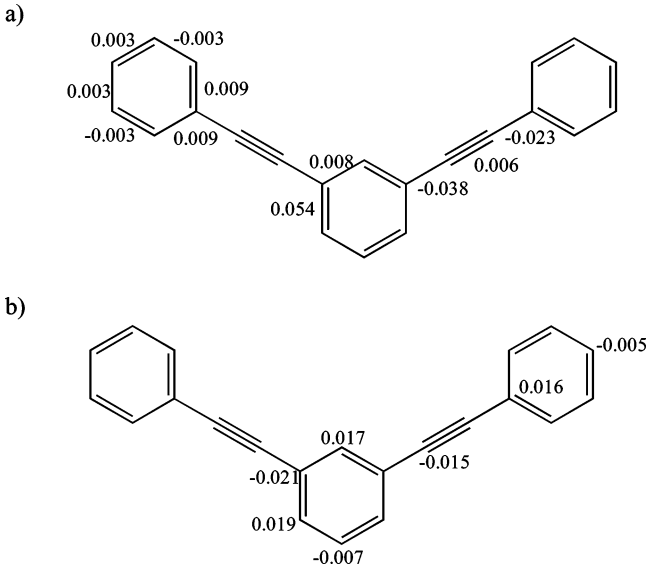

Figure 7. Changes in bond lengths (a) and Mulliken charges (b) at the optimized geometry on the emitting excited state (S_2) compared to the Franck−Condon geometry on the ground state. Bond lengths are in Å, and Mulliken charges are in au, summed over bonded hydrogen atoms. Only the most significant changes are shown for inequivalent atoms and bonds in C_{2v} symmetry. Excited state geometric relaxation is minimal, and the relaxed excited state has little charge-transfer character.

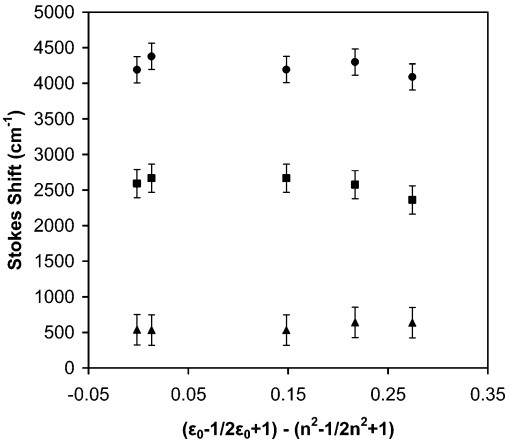

Figure 8. Dependence of experimental Stokes shift on solvent polarity for **1-Ph** (▲), **2-Ph** (■), and **3-Ph** (●).

many cases, the experimental Stokes shift, $\Delta\nu_{SS}$, is related to solvent polarity via the Lippert−Mataga reaction field,

$$\Delta\nu_{SS} = \frac{2\Delta\mu^2}{cha^3}\frac{\epsilon - 1}{2\epsilon + 1} - \frac{n^2 - 1}{2n^2 + 1} \qquad (6)$$

where ϵ is the static solvent dielectric constant, n is index of refraction, $\Delta\mu$ is the change in dipole moment, and a is the solute cavity.[55] A plot of eq 6 is shown in Figure 8, and the absence of any measurable solvent dependence suggests that there is no significant change in charge distribution between the ground and excited states. Therefore, the coupling in the emitting geometry is likely not due to a large charge-transfer character of the excited state.

4. Modeling the Origins of the Excitonic Coupling *V*. The previous sections have established that the experimental and ab initio results for the PA dendrons are consistent with a scenario where the excitonic coupling *V* changes from negligible in the absorbing geometry to large in the emitting geometry.

How can we understand this variation in terms of established theories[56] for electronic energy transfer? *V*, and thus the level splittings and energy transfer rates, can be calculated in a variety of ways using different approximations. In the crudest approximation, the Coulombic interaction of the two chromophore-localized transition densities is the only contribution to the matrix element *V* that is considered. When this Coulomb contribution is further approximated as the first nonvanishing term in a multipole expansion, the Förster theory is obtained.[4] Dexter later took higher-order multipole interactions into account,[57] but this approach is not expected to be rapidly convergent if the chromophores are close since the multipole expansion is only asymptotically convergent.[58] Krueger, Scholes, and Fleming have pointed out that multipole approximations may be avoided completely and that this can lead to significantly different results from point-dipole models.[59] It is worthwhile to reemphasize that all of these approaches are aimed at representing the same physical interaction—classical Coulombic interaction of the chromophore-localized transition densities. There are other contributions to the matrix element *V*, perhaps the most well-known being the exchange-like term highlighted by Dexter.[57] One of the more complete theoretical frameworks for understanding excitonic interactions so far introduced is that of Harcourt et al.[25,60,61] In this model, the Coulombic and exchange interactions, that is, the Förster and Dexter integrals, are clearly identified. However, the model goes further in also defining charge-transfer interactions, which can contribute to *V* and hence the exciton splitting. Although the outward appearance of these contributions is clearly charge transfer between chromophores, the model does not include state-specific orbital relaxation. Therefore, one should realize that it might be more appropriate to view these charge-transfer contributions as "through-bond" interactions in any particular case. We will use a modified Harcourt model to interpret the ab initio results and thus decompose the matrix element *V* into its constituent pieces. In this way, we will uncover the origin of the variable exciton coupling. For our purposes, it is sufficient to restrict our analysis to the **2-Ph** molecule, which illustrates the origin of the variable coupling.

The Harcourt model begins by defining a reduced chromophore-localized basis set. Specifically, the HOMO and LUMO orbitals localized on each chromophore are included. For two chromophores, this four orbital basis leads to four unique singly excited configurations: $|A^*B\rangle$, $|AB^*\rangle$, $|A^+B^-\rangle$, and $|A^-B^+\rangle$. The first two of these are the "covalent" configurations, which are usually considered in the theory of excitonic states.[4,47,57] The last two are "ionic" or charge-transfer configurations, and these configurations can introduce new contributions to the matrix element *V*, above and beyond the Förster and Dexter integrals. It is possible to extend this model to include dynamic electron correlation effects on the localized chromophores,[61] but we do not find that complication necessary in this case. We define orbitals *a* and *b* as the HOMO orbitals on chromophores A and B, respectively, and orbitals *a*′ and *b*′ as the LUMOs localized on chromophores A and B, respectively. With these definitions, the configurations included in the model are shown in Figure 9. The variable electronic coupling that we observe in the dendrons demands that we modify the Harcourt model somewhat. Thus, we provide a brief sketch of the relevant equations, pointing out differences as appropriate.

To map the results of the CASSCF calculations onto an exciton-like model, the orbitals must first be localized on the chromophores. We do this by orbital rotation within the active space, guaranteeing that the wave function would be unaffected

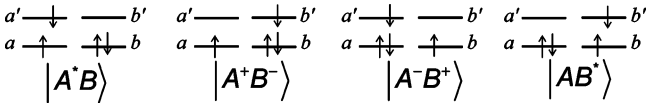

Figure 9. Diagram of the four configurations included in the exciton model. Orbitals *a* and *a*′ are localized on chromophore A, and orbitals *b* and *b*′ are localized on chromophore B.

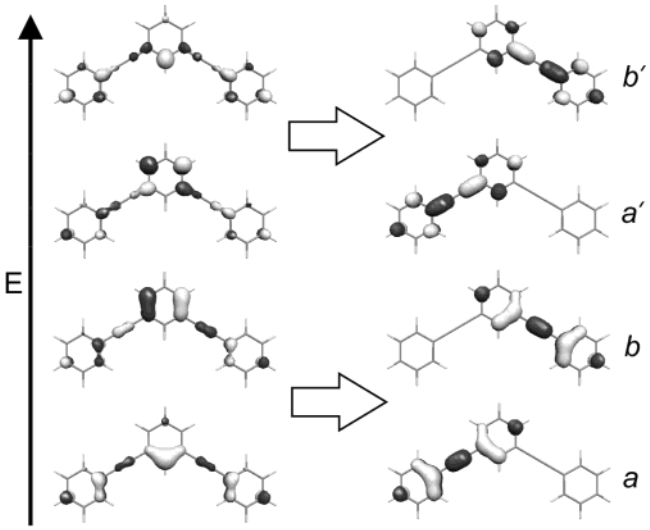

Figure 10. Delocalized orbitals (leftmost column) obtained from SA-6-CAS(12/12) for **2-Ph** and the DPA chromophore-localized orbitals obtained by orbital rotation (rightmost column). The chromophore-localized orbitals are used in the exciton model.

in a subsequent configuration interaction calculation including all of the electronic configurations. In the present case, we have found that this can be done by inspection, taking plus and minus combinations of the delocalized orbitals from the CASSCF calculations, as shown for **2-Ph** in Figure 10. This unitary transformation of the active space orbitals preserves their orthonormality, simplifying the model as pointed out below. A further point, which will become important in the following discussion, concerns the phases of the orbitals. We choose these phases to ensure that the Förster integral, $J = (aa'|bb')$, is positive. This is sufficient to fix the absolute signs of all of the terms that we discuss below, although it is of course only the relative signs that are important to the arguments. We further truncate the configuration basis to include only the four configurations of the Harcourt model as described above. In terms of the chromophore-localized orbitals, the wave functions are

$$\Psi_L = N(|A^*B\rangle + \lambda|A^+B^-\rangle + \mu|A^-B^+\rangle) \quad (7)$$

$$\Psi_R = N(|AB^*\rangle + \mu|A^+B^-\rangle + \lambda|A^-B^+\rangle) \quad (8)$$

where Ψ_L and Ψ_R are on the left and right chromophore, respectively, μ and λ are mixing coefficients, and *N* is the normalization factor

$$N = (1 + \lambda^2 + \mu^2)^{-1/2} \quad (9)$$

Because the orbitals that are the basis for our configurations are orthonormal, there is no overlap between different configurations. This leads to the simple form of the normalization seen here, compared to the more complicated form derived by Harcourt et al.[25] The coupling between the two chromophores becomes

$$T_{LR} = \langle \Psi_L | H - E_{RR} | \Psi_R \rangle = H_{LR} - S_{LR} E_{RR} \quad (10)$$

where E_{RR} is

$$E_{RR} = \langle \Psi_R | H | \Psi_R \rangle = \langle \Psi_L | H | \Psi_L \rangle \quad (11)$$

The energies of the two wave functions on the left- and right-hand sides of the molecule are equal because the chromophores are identical. The term $S_{LR}E_{RR}$ is subtracted from the off-diagonal matrix element H_{LR} because of the nonorthogonality of the constructed wave functions; although the orbitals are orthonormal, the configuration state functions Ψ_L and Ψ_R are not. In terms of the mixing coefficients, the matrix elements of eq 10 are given as

$$H_{LR} = N^2(V_{cc} + 2\mu V_{ic} + 2\lambda V'_{ic} + 2\lambda\mu E_i + (\lambda^2 + \mu^2)V_{ii}) \quad (12)$$

$$E_{RR} = N^2(E_c + (\lambda^2 + \mu^2)E_i + 2\lambda V_{ic} + 2\mu V'_{ic} + 2\lambda\mu V_{ii}) \quad (13)$$

$$S_{LR} = N^2(2\lambda\mu) \quad (14)$$

In these equations, V_{cc} and V_{ii} correspond to the coupling terms between the two covalent and ionic configurations, respectively. The energies E_c and E_i are those of the covalent and ionic configurations, and the terms V_{ic} and V'_{ic} are the couplings between one covalent configuration and each of the ionic configurations. The coupling T_{LR} is then

$$T_{LR} = N^2(V_{cc} + 2\mu V_{ic}(1 - 2N^2\lambda^2) + 2\lambda V'_{ic}(1 - 2N^2\mu^2) + V_{ii}(\lambda^2 + \mu^2 - 4N^2\lambda^2\mu^2) + 2\lambda\mu N^2(E_i - E_c)) \quad (15)$$

To determine the coupling quantitatively, the coefficients μ and λ must be found explicitly. One way of determining these coefficients is by finding the eigenvectors of the 3×3 Hamiltonian matrix including only the three configurations of interest, for example $|AB^*\rangle$, $|A^+B^-\rangle$, and $|A^-B^+\rangle$ for Ψ_R. The eigenvector of the mainly covalent state determines the values of the coefficients. This method is particularly useful when the coefficients are large and perturbation theory approximations are inaccurate. In many cases, however, the coefficients can be accurately determined through first-order perturbation theory corrections to the wave function formulated using nondegenerate perturbation theory. If the effects of the ionic configurations are small compared to the covalent configurations for Ψ_L and Ψ_R, the coefficients μ and λ can be approximated according to first-order perturbation theory. Using this and some other approximations motivated by perturbation theoretical arguments, Harcourt et al. derived[25] a simplified form of eq 15:

$$T_{LR} \approx N^2\left(V_{cc} - \frac{2V_{ic}V'_{ic}}{E_i - E_c}\right) \quad (16)$$

We use the variational expression in eq 15 for our calculations but include the perturbation expression for completeness and because it is helpful for understanding the origin of the different terms. The coupling between the two chromophores can be interpreted as having two distinct parts. The first term in parentheses in eq 16, V_{cc}, includes the Coulomb and exchange integrals corresponding to the terms seen in the formulations of Förster and Dexter. When the term V_{cc} is calculated explicitly, it can be expressed as

$$V_{cc} = \langle A^*B | H | AB^* \rangle = 2(a'a|bb') - (a'b'|ba) = 2J - K \quad (17)$$

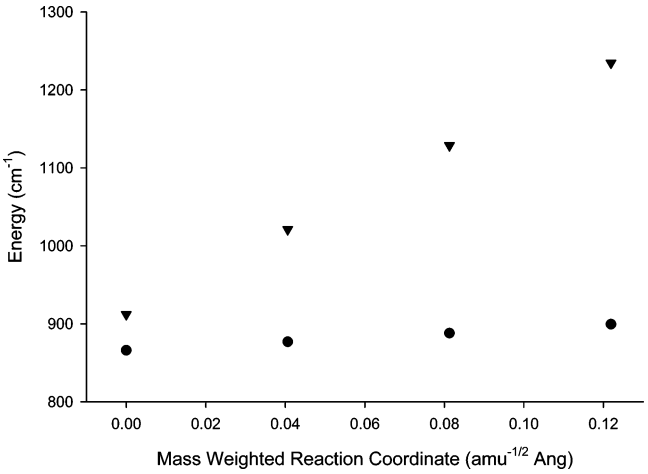

Figure 11. Variations, including the normalization factor N^2, in the through-space (V_{cc}) term (●) and the charge-transfer term (▼) of eq 15 as a function of geometry. The path shown is a linear interpolation between the absorbing geometry (left) and emitting geometry (right).

using standard notation for two-electron integrals,[62] where J is the Förster Coulomb integral and K is the Dexter exchange integral.[63] The second term in parentheses in eq 16 includes the coupling related to the involvement of ionic configurations. This term could be seen as implying slight charge-transfer or polarization character of the state or alternatively as implying through-bond character. The consideration of the normalization factor N^2 becomes increasingly important as the contributions from the ionic configuration increase, as seen in eq 9. In the molecules studied here, the values of λ and μ can be quite significant, leading to values of N^2 that differ significantly from unity. Therefore, in our calculations, the normalized coupling is always computed.

Having laid out the basic equations of the Harcourt model, we now apply them to the **2-Ph** molecule. These calculations do not include dynamic electron correlation and hence are at a lower level of theory than those in section 2. However, since these calculations show all of the same qualitative features as the more sophisticated calculations for **(1−3)-H**, we believe that they capture the essence of the phenomena for all of the molecules. The ground and excited state geometries are obtained by optimizing using C_{2v} symmetry and SA-1-CASSCF(4/4) and SA-5-CASSCF(4/4) wave functions, respectively. A SA-6-CASSCF(12/12) calculation in C_s symmetry is used to obtain delocalized orbitals. Linear combinations of four of these orbitals are taken to form two localized orbitals on each branch of the molecule as seen in Figure 11. These orbitals are used to construct the four configurations of the Harcourt model, and the resulting Hamiltonian matrix is constructed. A linearly interpolated path in Cartesian coordinates is calculated between the absorbing and emitting geometries for **2-Ph**, and the orbitals and Hamiltonian matrix are recalculated for each of these points. Because the geometric relaxation on the excited state is so small, the results are not sensitive to the details of how this path is constructed.

The coupling T_{LR} is found using eq 15, as opposed to the approximate perturbation result in eq 16. Nevertheless, it is instructive to separate the terms in eq 15 according to the decomposition implied by eq 16. In particular, the first term in parentheses of eq 15 is denoted the through-space term, and all remaining terms are denoted the charge-transfer contribution. The variation in the through-space and charge-transfer terms in eq 15 as a function of geometry is shown in Figure 11. The through-space term, V_{cc}, remains nearly constant as the geometry

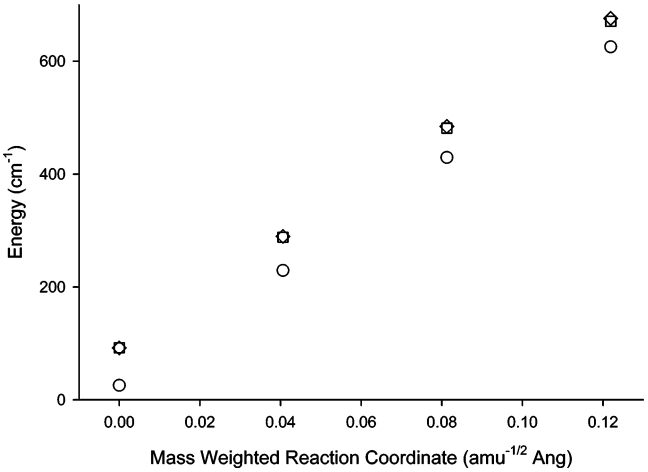

Figure 12. Energy splitting in wavenumbers along the reaction coordinate between the absorbing and emitting geometries. The complete CAS (○), small Hamiltonian (◇), and Harcourt model ($2T_{LR}$) (□) results are shown.

relaxes, while the charge-transfer term increases from the absorbing to emitting geometries. Interpreting the result using eq 16, we see that the through-space and charge-transfer terms cancel each other for these geometries of **2-Ph** because they are both positive; this is easily understood from the negative sign in eq 16. At the absorbing geometry, the magnitude of the two terms is similar, leading to a normalized coupling of -46 cm^{-1}. At the emitting geometry, however, the second term involving the ionic configurations has become larger while the first term has remained essentially unchanged, leading to a normalized coupling of -335 cm^{-1}. This change in the coupling as a function of geometry leads to a change in the energy splitting between the two nearly degenerate states upon excited state relaxation. Figure 12 shows the energy splitting over the linearly interpolated path between the absorbing and emitting geometries. The result of the complete CASSCF calculation is compared to that obtained from exact diagonalization of the truncated basis Hamiltonian including only the four Harcourt model configurations and the ground state configuration. The energy splittings predicted by eq 15 are also shown, where the splitting is equal to twice the coupling. The energy splittings from the complete CASSCF and truncated basis Hamiltonian calculations agree to within about 50 cm^{-1}, indicating that the truncated basis Hamiltonian provides an excellent description of the exciton splitting. The energy splittings deduced from eq 15 differ from those predicted by the truncated basis Hamiltonian by at most 5 cm^{-1}, demonstrating that the modified Harcourt model of eq 15 includes the important characteristics of the small Hamiltonian. In addition to their failures in properly representing the Förster integral, point-dipole models neglect the Dexter and charge-transfer contributions to the exciton splitting. Given the results of our analysis, we can now understand how each of these failures contributes to the inability of a crude exciton model to describe the observations in these dendrons. The traditional J and K terms cancel with the ionic terms in the coupling at the absorbing geometry leading to a very small coupling. However, as the geometry relaxes on the excited state, the ionic coupling term increases significantly. Because the geometry has not changed much, the J and K terms are virtually unaffected by this relaxation and no longer serve to balance the ionic coupling term. This results in a large apparent coupling increase from the absorbing geometry to the emitting geometry.

The sensitivity of the ionic terms to geometry in the face of insensitivity of the J and K terms is at first sight somewhat puzzling. Additionally, we recall that experiments find no indication of charge transfer in the excited states of these molecules. However, these puzzles really arise from a misnaming of the charge-transfer term, which we have alluded to above. In the limited basis of the Harcourt model, where a single set of orbitals is used for all states, any state-specific orbital relaxation can only be described by ionic configurations. Thus, the charge-transfer term in this case is essentially a "through-bond" interaction, reflecting the change in electronic structure as cumulenic resonance structures become more favored.[64] As seen in eq 16, the through-space term is V_{cc}, and the through-bond term includes the matrix elements V_{ic} and V'_{ic}. The expression for the through-space term includes only the two-electron integrals shown in eq 17, while the expressions for V_{ic} and V'_{ic} include one-electron as well as two-electron integrals. The geometry distortions are slight, which leads to the relatively small changes in the values of the two-electron integrals. These slight geometrical distortions, however, significantly change the bond orders, leading to a cumulenic structure. Such changes in bonding are expected to have a much greater impact on the one-electron integrals, especially the kinetic energy terms.[65,66] As a result, the through-space term, which depends only on two-electron integrals, is changed very little as a function of the relaxation of the geometry, while the through-bond term, which includes one-electron integrals, changes significantly along the relaxation coordinate. In this interpretation, there is no mystery as to the sensitivity of this term to cumulenic geometry distortions nor in the absence of an influence of solvent polarity on the observed variable exciton coupling.

TABLE 3: Coupling Terms and J and K Integrals in cm^{-1} for 2-Ph and P2-Ph[a]

	2-Ph		P2-Ph	
	absorbing	emitting	absorbing	emitting
J	1364	1420	1021	1471
K	1804	1862	−1377	−794
$2J - K$	924	978	3419	3736
T_{LR}	−46	−335	6441	8265
point-dipole	1361		1028	

[a] The point-dipole model coupling values are calculated using Equation 6. These point-dipole values correspond to $2J$.

To further understand why the two coupling terms nearly cancel in the absorbing geometry of **2-Ph**, the para-substituted isomer 1,4-bis(phenylethynyl)benzene (**P2-Ph**) is examined. The absorbing and emitting geometries are obtained using SA-1-CASSCF(4/4) and SA-2-CASSCF(4/4) wave functions in C_s symmetry. The ground state geometry has D_{2h} symmetry, so both chromophores are identical. In the emitting excited-state minimum, however, the two chromophores no longer have the same geometry. The delocalized orbitals from a SA-4-CASSCF-(4/4) calculation in C_s symmetry are rotated to form the orbitals localized on each chromophore. The sign of the coupling term involving the ionic terms has changed in **P2-Ph** so that the terms add instead of cancel. Additionally, the sign of the entire coupling is positive. The coupling is about 6400 cm^{-1} in the absorbing geometry, and the V_{cc} and ionic terms contribute nearly equally to the coupling. Because of the reduced symmetry in the emitting geometry, the assumption that the two chromophores are identical is no longer valid. Therefore, the coupling equations are used without this assumption.[61] The two terms again add to result in a coupling of about 8300 cm^{-1}. The coupling in these molecules is large in the absorbing geometry and remains large in the emitting geometry. In Table 3, we compare the J and K integrals for the absorbing and emitting states of **2-Ph** and **P2-Ph**. The quantity $2J - K$ results

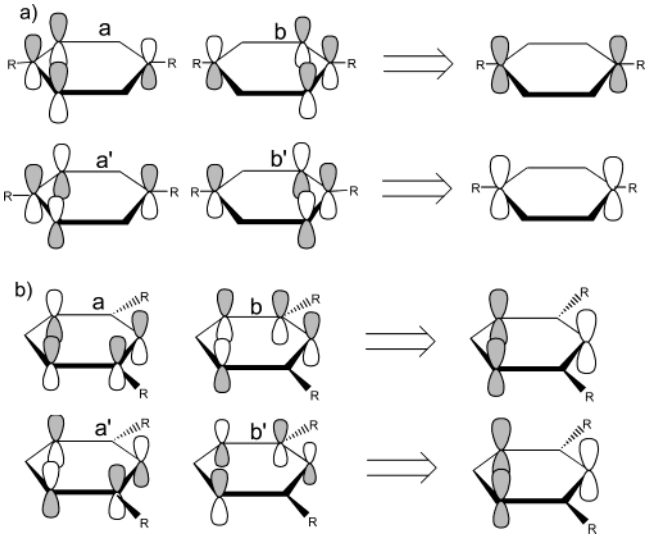

Figure 13. Charge densities from Dexter exchange integral, $K = (a'b'|ba)$, for (a) para-substituted dimer and (b) meta-substituted dimer. We point out especially the difference in the relative phases of the interacting charge densities in the para- and meta-substituted cases. This shows that a negative value is expected for the para-substituted dimer, while a positive value should be expected for the meta-substituted dimer.

in the first coupling term, V_{cc}. As seen in Table 3, the value for J from the ab initio calculations is 1364 cm^{-1} in the ground state and 1420 cm^{-1} in the excited state for **2-Ph**. The values of J are 939 and 1466 cm^{-1} in the absorbing and emitting geometries, respectively, for **P2-Ph**. Because of the sign change of the K integral between **2-Ph** and **P2-Ph**, the quantity $2J - K$ is about 4 times as large in the para-substituted molecules as in the meta-substituted ones. This large Coulomb coupling dominates the charge-transfer term and leads to the large overall coupling seen in **P2-Ph** compared to **2-Ph**.

A close examination of the Coulomb terms J and K reveals some interesting trends. The values of J for the meta-substituted and para-substituted molecules are similar for the two geometries of each of the molecules. In all cases, the sign of J is positive and the magnitude is about 1000 cm^{-1}. The Coulomb integral J can be related to the point-dipole coupling, $V_{point-dipole}$, by the relationship $2J \approx V_{point-dipole}$. The point-dipole model gives a value of $V \approx 1400$ cm^{-1}, which is smaller by about a factor of 2 than that predicted by the Coulomb integral. However, due to the $1/r^3$ dependence of the point-dipole coupling, the coupling $V_{point-dipole}$ can change by a factor of 2 with only moderate changes in the distance between the dipoles, and this discrepancy is not surprising. The surprise is that the value of the exchange integral K is very different for the para- and meta-substituted molecules. For **2-Ph**, the magnitude of K is unchanged between the absorbing and emitting geometries and the sign is always positive. For **P2-Ph**, however, the magnitude of K in the absorbing geometry is similar to that in **2-Ph**, but the sign is negative. In the emitting geometry, the magnitude of K decreases, but the sign remains negative. To physically understand the change in sign of K, we examine the different characters of the overlap integrals in Figure 13. The exchange integral is defined as

$$(ij|kl) = \int d\mathbf{r}_1\, d\mathbf{r}_2\, \phi_i^*(\mathbf{r}_1)\phi_j(\mathbf{r}_1)\frac{1}{r_{12}}\phi_k^*(\mathbf{r}_2)\phi_l(\mathbf{r}_2) \qquad (18)$$

Therefore, the product (or transition density) of the two orbitals i and j, along with the transition density of orbitals k and l, is used to find the value of the exchange integral. In the para-substituted case (Figure 13a), the phases of the two transition densities are different. For the meta-substituted case, however, the phases are the same. The introduction of this phase difference leads to the change in sign of K from **2-Ph** to **P2-Ph**.

Discussion and Conclusion

The results discussed in this paper have significant implications for the design and analysis of conjugated networks based on phenylacetylene units. First, the assumption that meta-conjugation effectively prevents electronic communication between dendrimer arms is only true at the ground state geometry of these molecules. The fact that the absorption spectrum undergoes little change as more segments are added is due to a fortuitous cancellation of coupling terms and not, as previously assumed, due to an intrinsically small coupling between the arms. When this balance is upset by nuclear relaxation on the excited-state potential energy surface, strong excitonic coupling transforms the electronic structure from quasi-degenerate, localized states to delocalized states shifted in energy by 2000 cm^{-1} or more. Due to the lack of coupling in the ground state, the absorption is localized on the DPA chromophore for **(1−3)-Ph**, as well as for the higher generation dendrimers. As a result of the strong coupling, which turns on after the excitation, the emission shifts by about 2000 cm^{-1} from **1-Ph** to **2-Ph** to **3-Ph** but does not shift any further with the high generation dendrimers. Therefore, the delocalized states for the emission change as a function of the increased meta-substitution. The emissive behavior of the higher generation dendrimers indicates that the delocalized states may have the same character as that of the delocalized emitting state in **3-Ph**.

Thus meta-conjugation by itself is not necessarily sufficient to prevent electronic coupling in the excited state. Similar behavior has been observed and discussed in the quite different context of benzene photochemistry by Zimmerman.[67] Of course, once the true nature of the excited state has been determined, its energy transfer dynamics may be analyzed in terms of a reduced model that treats the quantum mechanical nature of the energy transfer through a network of excitonically coupled sites.[68−71] However, such a model should also be cognizant of the changes in electronic coupling that occur in the excited-state manifold for these molecules.

In fact, it is possible that the relaxation-induced coupling is beneficial for the function of these systems as light harvesters. This comes about through several effects. First, the excited states of the multiply branched PA dendrons are shifted lower in energy, and this is apparently enough to turn off the fast internal conversion pathway that is observed in monomeric DPA.[40−42] Similar effects have also been observed in phenylene−vinylene analogues of the **-Ph** molecules, where additional branches lead to emission shifts and a decreased nonradiative relaxation rate.[72] In this case, the photoisomerization of *trans*-stilbene is suppressed by adding more phenylene−vinylene groups at the meta positions of a central benzene. In addition to allowing the excited-state population to avoid internal conversion pathways, the new states also have smaller emission probabilities due to their negative coupling constant. A lower radiative rate means that less energy is lost to spontaneous emission. In this sense, the dendrons are similar to the well-known H-aggregates,[47] in that they can store energy in a weakly allowed, low-lying state where it can eventually be channeled to do useful chemistry. The unique feature of the meta-linked phenylacetylenes is that they do not have the blue-shifted absorption spectrum usually associated with H-aggregates; they only manifest their H-

aggregate character after absorbing a photon. Thus it is possible to build an aggregate that has the strong, unshifted absorption of the monomer building block but with a relaxed excited state that enhances energy transfer due to its weak emission and strong intersegment coupling. Through vibrational relaxation and geometry changes, the molecule can change from being a good absorber to a good energy transfer medium. This ability to change from weak to strong coupling makes the PA dendrimers unique in the context of multichromophoric dendrimers, most of which are completely in the weakly coupled limit of Förster energy transfer.

This work shows that the combination of organic synthesis, experimental spectroscopy, and detailed analysis using ab initio quantum theory can quantitate the electronic coupling that determines the excited-state structure and energy transfer in conjugated supramolecular systems. Our decomposition of the ab initio results in terms of the Coulomb *J* and *K* integrals and the charge-transfer term provides a conceptual framework for the analysis of the systems. The finding that a geometry-dependent exciton coupling, *V(Q)*, determines the excited-state electronic structure demonstrates that our approach can yield novel insights into the structure and dynamics of such systems. Questions of how the coupling depends on chemical substitution and molecular vibrational structure remain to be answered. Nevertheless, this achievement bodes well for the development of physical and theoretical methods to provide the basis for a systematic approach for the rational design of high-efficiency light-harvesting molecular assemblies.

Acknowledgment. This work was supported by DOE Grant DEFG-01ER15270. T.J.M. is a Packard Fellow, Dreyfus Teacher-Scholar, and UIUC Petit Scholar. C.J.B. is an Alfred P. Sloan Research Fellow. A.L.T. is a grateful recipient of an NSF predoctoral fellowship and UIUC Distinguished fellowship.

Supporting Information Available: Synthetic procedures, detailed derivations of equations used in the modified Harcourt model, Cartesian coordinates of geometries discussed in the text, and detailed results of electronic structure calculations including the truncated Hamiltonian matrices used to interpret the geometry-dependent exciton coupling. This material is available free of charge via the Internet at http://pubs.acs.org.

References and Notes

(1) Adronov, A.; Frechet, J. M. J. *Chem. Commun.* **2000**, 1701.
(2) Speiser, S. *Chem. Rev.* **1996**, *96*, 1953.
(3) Joilbois, F.; Bearpark, M. J.; Robb, M. A. *J. Phys. Chem.* **2002**, *106A*, 4358.
(4) Forster, T. Delocalized Excitation and Excitation Transfer. In *Modern Quantum Chemistry*; Sinanoglu, O., Ed.; Academic Press: New York, 1965; Vol. 3; p 93.
(5) Mukamel, S.; Franchi, D. S.; Loring, R. F. *Chem. Phys.* **1988**, *128*, 99.
(6) Pullerits, T.; Sundstrom, V. *Acc. Chem. Res.* **1996**, *29*, 381.
(7) Hu, X.; Ritz, T.; Damjanovic, A.; Schulten, K. *J. Phys. Chem.* **1997**, *101B*, 3854.
(8) Agarwal, R.; Rizvi, A. H.; Prall, B. S.; Olsen, J. D.; Hunter, C. N.; Fleming, G. R. *J. Phys. Chem.* **2002**, *106A*, 7573.
(9) Adronov, A.; Gilat, S. L.; Frechet, J. M. J.; Ohta, K.; Neuwahl, F. V. R.; Fleming, G. R. *J. Am. Chem. Soc.* **2000**, *122*, 1175.
(10) Neuwahl, F. V. R.; Righini, R.; Adronov, A.; Malenfant, P. R. L.; Frechet, J. M. J. *J. Phys. Chem.* **2001**, *105B*, 1307.
(11) Ranasinghe, M. I.; Wang, Y.; Goodson, T., III *J. Am. Chem. Soc.* **2003**, *125*, 5258.
(12) Varnavski, O.; Samuel, I. D. W.; Palsson, L.-O.; Beavington, R.; Burn, P. L.; Goodson, T. *J. Chem. Phys.* **2002**, *116*, 8893.
(13) Meskers, S. C. J.; Bender, M.; Hubner, J.; Romanovskii, Y. V.; Oestreich, M.; Schenning, A. P. H. J.; Meijer, E. W.; Bassler, H. *J. Phys. Chem.* **2001**, *105A*, 10220.
(14) Maus, M.; De, R.; Lor, M.; Weil, T.; Mitra, S.; Wiesler, U. M.; Herrmann, A.; Hofkens, J.; Vosch, T.; Mullen, K.; Schryver, F. C. D. *J. Am. Chem. Soc.* **2001**, *123*, 7668.
(15) Yeow, E. K. L.; Ghiggino, K. P.; Reek, J. N. H.; Crossley, M. J.; Bosman, A. W.; Schenning, A. P. H. J.; Meijer, E. W. *J. Phys. Chem.* **2000**, *104B*, 2596.
(16) Varnavski, O. P.; Ostrowski, J. C.; Sukhomlinova, L.; Twieg, R. J.; Bazan, G. C.; Goodson, T., III *J. Am. Chem. Soc.* **2002**, *124*, 1736.
(17) Melinger, J. S.; Pan, Y.; Kleiman, V. D.; Peng, Z.; Davis, B. L.; McMorrow, D.; Lu, M. *J. Am. Chem. Soc.* **2002**, *124*, 12002.
(18) Tretiak, S.; Chernyak, V.; Mukamel, S. *J. Phys. Chem.* **1998**, *102B*, 3310.
(19) Shortreed, M. R.; Swallen, S. F.; Shi, Z. Y.; Tan, W.; Xu, Z.; Devadoss, C.; Moore, J. S.; Kopelman, R. *J. Phys. Chem.* **1997**, *101B*, 6318.
(20) Kopelman, R.; Shortreed, M.; Shi, Z. Y.; Tan, W.; Xu, Z.; Moore, J. S.; Bar-Haim, A.; Klafter, J. *Phys. Rev. Lett.* **1997**, *78*, 1239.
(21) Kleiman, V. D.; Melinger, J. S.; McMorrow, D. *J. Phys. Chem.* **2001**, *105B*, 5595.
(22) Devadoss, C.; Bharathi, P.; Moore, J. S. *J. Am. Chem. Soc.* **1996**, *118*, 9635.
(23) Gaab, K. M.; Thompson, A. L.; Xu, J.; Martinez, T. J.; Bardeen, C. J. *J. Am. Chem. Soc.* **2003**, *125*, 9288.
(24) Beljonne, D.; Pourtois, G.; Silva, C.; Hennebicq, E.; Herz, L. M.; Friend, R. H.; Scholes, G. D.; Setayesh, S.; Mullen, K.; Bredas, J. L. *Proc. Natl. Acad. Sci. U.S.A.* **2002**, *99*, 10982.
(25) Harcourt, R. D.; Scholes, G. D.; Ghiggino, K. P. *J. Chem. Phys.* **1994**, *101*, 10521.
(26) Xu, Z.; Kahr, M.; Walker, K. L.; Wilkins, C. L.; Moore, J. S. *J. Am. Chem. Soc.* **1994**, *116*, 4537.
(27) Potts, W. J., Jr. *J. Chem. Phys.* **1952**, *20*, 809.
(28) Lim, S.-H.; Bjorklund, T. G.; Gaab, K. M.; Bardeen, C. J. *J. Chem. Phys.* **2002**, *117*, 454.
(29) Volkmer, A.; Hatrick, D. A.; Birch, D. J. S. *Meas. Sci. Technol.* **1997**, *8*, 1339.
(30) Werner, H.-J.; Knowles, P. J.; Lindh, R.; Schuetz, M.; et al. MOLPRO, Version 2002.2, a package of ab initio programs. (Available via the Internet at http://www.molpro.net.)
(31) Werner, H.-J.; Knowles, P. J. *J. Chem. Phys.* **1985**, *82*, 5053.
(32) Knowles, P. J.; Werner, H.-J. *Chem. Phys. Lett.* **1985**, *115*, 259.
(33) Roos, B. O. *Adv. Chem. Phys.* **1987**, *69*, 399.
(34) Hehre, W. J.; Ditchfield, R.; Pople, J. A. *J. Chem. Phys.* **1972**, *56*, 2257.
(35) Andersson, K.; Malmqvist, P.-A.; Roos, B. O.; Sadlej, A. J.; Wolinski, K. *J. Phys. Chem.* **1990**, *94*, 5483.
(36) Celani, P.; Werner, H.-J. *J. Chem. Phys.* **2000**, *112*, 5546.
(37) Hariharan, P. C.; Pople, J. A. *Theor. Chim. Acta* **1973**, *28*, 213.
(38) *Jaguar*, 4.1 ed.; Schrodinger, Inc.: Portland, OR, 2000.
(39) Shortreed, M. R. Ph.D. Thesis, University of Michigan, Ann Arbor, MI, 1996.
(40) Hirata, Y.; Okada, T.; Mataga, N.; Nomoto, T. *J. Phys. Chem.* **1992**, *96*, 6559.
(41) Ferrante, C.; Kensy, U.; Dick, B. *J. Phys. Chem.* **1993**, *97*, 13457.
(42) Zimdars, D.; Francis, R. S.; Ferrante, C.; Fayer, M. D. *J. Chem. Phys.* **1997**, *106*, 7498.
(43) Lakowicz, J. R. *Principles of Fluorescence Spectroscopy*; Plenum Press: New York, 1983.
(44) Higgins, J.; Ernst, W. E.; Callegari, C.; Reho, J.; Lehmann, K. K.; Scholes, G.; Gutowski, M. *Phys. Rev. Lett.* **1996**, *77*, 4532.
(45) King, G. W.; So, S. P. *J. Mol. Spectrosc.* **1971**, *37*, 543.
(46) This systematic offset is at least partially because we compute the experimental Stokes shift as a difference of the 0−0 absorption and emission lines, while the theoretical value is reported as a difference of the vertical excitation and emission energies. Detailed theoretical modeling of the absorption and emission electronic spectra would be required to improve the agreement further.
(47) Kasha, M.; Rawls, H. R.; El-Bayoumi, M. A. *Pure Appl. Chem.* **1965**, *11*, 371.
(48) Czikklely, V.; Forsterling, H. D.; Kuhn, H. *Chem. Phys. Lett.* **1970**, *6*, 207.
(49) Evans, C. E.; Song, Q.; Bohn, P. W. *J. Phys. Chem.* **1993**, *97*, 12302.
(50) Halasinski, T. M.; Weisman, J. L.; Ruiterkamp, R.; Lee, T. J.; Salama, F.; Head-Gordon, M. *J. Phys. Chem.* **2003**, *107A*, 3660.
(51) El-Sayed, M. A.; Robinson, G. W. *Mol. Phys.* **1961**, *4*, 273.
(52) Borst, D. R.; Chou, S. G.; Pratt, D. W. *Chem. Phys. Lett.* **2001**, *343*, 289.
(53) Harigaya, K. *Chem. Phys. Lett.* **1999**, *300*, 33.
(54) Nakano, M.; Fujita, H.; Takahata, M.; Yamaguchi, K. *J. Am. Chem. Soc.* **2002**, *124*, 9648.
(55) Maroncelli, M.; Fleming, G. R. *J. Chem. Phys.* **1987**, *86*, 6221.
(56) Scholes, G. D. *Annu. Rev. Phys. Chem.* **2003**, *54*, 57.
(57) Dexter, D. L. *J. Chem. Phys.* **1953**, *21*, 836.

(58) Jackson, J. D. *Classical Electrodynamics*, 3rd ed.; Wiley: New York, 1999.
(59) Krueger, B. P.; Scholes, G. D.; Fleming, G. R. *J. Phys. Chem.* **1998**, *102B*, 5378.
(60) Scholes, G. D.; Harcourt, R. D.; Ghiggino, K. P. *J. Chem. Phys.* **1995**, *102*, 9574.
(61) Scholes, G. D.; Harcourt, R. D. *J. Chem. Phys.* **1996**, *104*, 5054.
(62) Szabo, A.; Ostlund, N. S. *Modern Quantum Chemistry*; McGraw-Hill: New York, 1989.
(63) Murrell, J. N.; Tanaka, J. *Mol. Phys.* **1963**−**4**, *7*, 363.
(64) Ohanessian, G.; Hiberty, P. C. *Chem. Phys. Lett.* **1987**, *137*, 437.
(65) Ruedenberg, K. *Rev. Mod. Phys.* **1962**, *34*, 326.
(66) Wilson, C. W.; Goddard, W. A. *Chem. Phys. Lett.* **1970**, *5*, 45.
(67) Zimmerman, H. E. *J. Am. Chem. Soc.* **1995**, *117*, 8988.
(68) Bar-Haim, A.; Klafter, J. *J. Phys. Chem.* **1998**, *102B*, 1662.
(69) Kirkwood, J. C.; Scheurer, C.; Chernyak, V.; Mukamel, S. *J. Chem. Phys.* **2001**, *114*, 2419.
(70) Raychaudhuri, S.; Shapir, Y.; Chernyak, V.; Mukamel, S. *Phys. Rev. Lett.* **2000**, *85*, 282.
(71) Scholes, G. D.; Jordanides, X. J.; Fleming, G. R. *J. Phys. Chem.* **2001**, *105B*, 1640.
(72) Meier, H.; Zertani, R.; Noller, K.; Oelkrug, D.; Krabichler, G. *Chem. Ber.* **1986**, *119*, 1716.